Supplementary Material for manuscript 'Evidence for focused magmatic accretion at segment centers from lateral dike injections captured beneath the Red Sea rift in Afar'

by Keir et al.

Seismic methods

Stations

From April to August 2006, seismicity in Afar was recorded by a temporary network of 4 broadband, 3 component Güralp 6TD seismographs deployed at distances of 50-150 km from the Dabbahu segment (Table SM1) (Fig. 1). Stations recorded continuous data at a sample rate of 50 Hz. Data is supplemented by continuous records from the nearest permanent short period, 3 component instruments located in Dese (Ethiopia) and Arta (Djibouti).

Epicenters and magnitude

Earthquakes were identified by manual inspection of all available continuous data, and for those recorded at 3 or more stations arrival times of P- and S-phases were measured. Earthquake epicenters were derived using a 3-layer 1-D velocity model constrained from controlled source experiments in northern Afar by Makris and Ginzburg (1987). Epicenters have estimated uncertainties of between ~1-5 km, but due to the lack of seismic stations near the Dabbahu segment, earthquake depths cannot be reliably constrained from arrival time data alone. However, depth constrained rift axis seismicity near Semera and beneath the Dabbahu segment shows an ~8 km thick seismogenic layer (Gresta et al., 1997; Ebinger et al., 2008). We fixed earthquake depths to 5 km, and epicenters derived using depths fixed in the range 1-10 km show no discernible difference from those presented. Earthquake magnitude was

measured using the maximum body-wave displacement amplitudes on a simulated Wood-Anderson seismograph and distance correction terms of Keir et al., (2006), appropriate for Ethiopia. Seismic moment is estimated from earthquake magnitude using the empirical m_b-m_o relationship established for northeast Afar by Hofstetter and Beyth (2003).

Along-axis position of seismicity

Note that the seismic stations in Abala and Semera, as well as the axis of the Dabbahu segment, align along a NW oriented straight-line profile (Fig. 1). Such geometry allows the along-axis position of rift zone seismicity to be directly estimated by subtracting the P-wave arrival times of each earthquake recorded at Abala from the P-wave arrival time recorded at Semera. The resulting "2-D" earthquake location has precision limited only by accuracy of arrival time measurements and removes all errors in epicentral location introduced by a poorly constrained velocity models and sub-optimal azimuthal ray coverage. Differences in P-wave arrival times are plotted against time (Fig. 3).

Because Abala and Semera are large distances (~140 and ~70 km respectively) from the center of the Dabbahu segment, the difference in P-wave arrival time measured at these stations is highly sensitive to changes in epicentral locations and relatively unaffected by variations in earthquake depth. For example, a 3 km northward shift of epicenter along the rift axis functions to decrease the arrival time of the P-wave at Abala by 0.5 s, but also increases the arrival time in Semera by 0.5 s resulting in a 1 s measured change in difference of P-wave arrival time at the two stations. This is above the maximum 0.2 s measurement error in arrival time of the P-waves. However, any shift in earthquake depth functions to change the arrival

times of P-waves at the two distant stations in the same sense, producing almost no change in difference of P-wave arrival time at the two distant stations.

Name	Lat.	Long.	Elev. (m)
Abale	13.35282	39.76271	1465
Afdera	13.20733	40.85717	-83
Semera	11.79179	41.00344	439
Silsa	12.40695	41.18790	477
Dese	11.12000	39.64000	1950
ATD	11.53000	42.84700	100

Table SM1: Seismic station names and locations

Date	Time (GMT)	Lat.	Long.	m_b
2006/06/17	14:33:32.39	12.24	40.51	4.4
2006/06/17	14:45:15.93	12.40	40.80	4.6
2006/06/17	15:42:59.12	12.29	40.62	3.9
2006/06/17	16:20:40.51	12.31	40.54	4.5
2006/06/17	16:53:10.60	12.24	40.53	4.3

Table SM2: Earthquakes reported by National Earthquake Information Center (NEIC) located in the Dabbahu rift during 2006.

Radar interferometry methods

Following the September 2005 dike intrusion, regular Advanced Satellite Aperture Radar (ASAR) acquisitions were scheduled over the Dabbahu segment using the European Space Agency (ESA) ENVISAT satellite. We use images acquired on ascending track 300 (12 June, 17 July, 21 August 2006) and descending track 49 (20 May, 24 June, 29 July 2006) to produce interferograms that isolate the deformation associated with the dikes intruded on 17 June and 25 July 2006. All of the interferograms were processed using the JPL/Caltech ROI_PAC software (Rosen et al, 2004). Topographic corrections were made using a 3 arc-second, (90m) digital elevation model (DEM) generated by the NASA Shuttle Radar Topography Mission (SRTM) (Farr & Kobrick, 2000); interferograms were filtered using a power spectrum filter (Goldstein & Werner, 1998), unwrapped using the branch cut algorithm (Goldstein et al., 1988), and sampled using the Quadtree method (e.g. Jonsson et al., 2000).

To determine the geometry of the dikes, they were initially modeled as rectangular dislocations in an elastic half space, with uniform opening, following the formulations of Okada (1985). Subsequently, the tensile dislocations were broken into rectangular patches of 1 x 1 km size and a smooth distribution of opening was determined that best fit the observed line-of-sight deformation. Normal faults, bounding the central subsiding graben, were added to represent faults observed in the field. Full details of the method used are presented in Hamling et al. (2008, in review), and full details of InSAR observations and modeling for the June and July 2006 dikes are presented below.

June 2006 dike

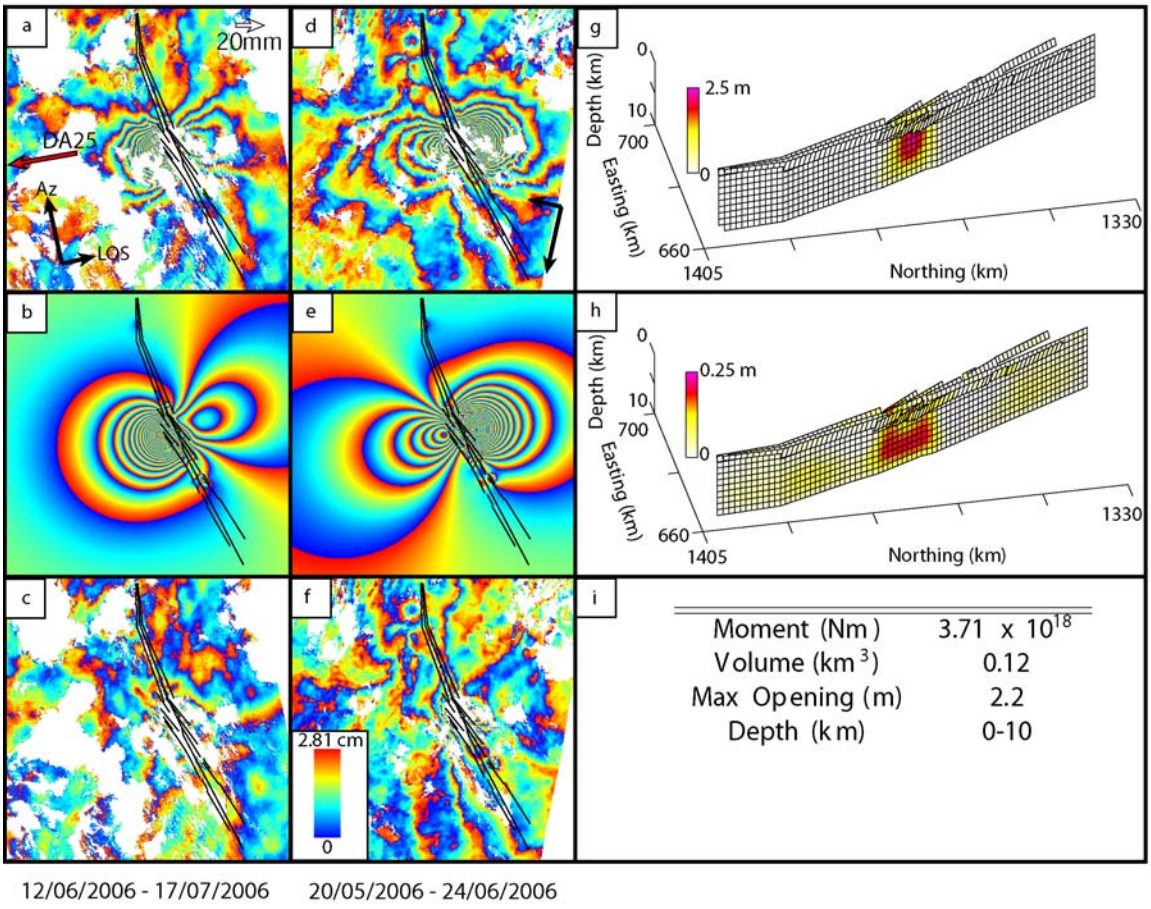

Figure SM1: Observed and modeled deformation for the June 2006 dike intrusion. a) observed, b) modeled, c) residual ascending interferograms. c) observed, d) modeled, e) residual descending interferograms, f) Best-fit dike model, h) 1-σ errors, i) dike statistics.

Satellite radar images acquired on May 20 and June 24 from track 464 were used to construct a 35-day descending interferogram (Fig. SM1d). A large baseline of ~1200 m does not allow us to form the ascending interferogram using images from track 300 acquired on June 12 and July 17. Instead, we used the ascending interferogram for June 12 to August 21, which includes deformation from dikes during both June and July. In order to isolate the signal for

the June dike, the deformation associated with the July dike was removed by subtracting the 35-day ascending interferogram from track 300 for July 17 to August 21. The resulting interferogram is shown is (Fig. SM1a). Continuous global positioning system (cGPS) displacements recorded during June 2006 at six sites installed around the Dabbahu segment were incorporated into the deformation data. The closest GPS station to the June 2006 dike was located 25 km west of the rift axis, and recorded a westward displacement of 47 mm.

The observed surface deformation patterns are in agreement with the displacement field expected of a dike. The best-fitting model (Fig. SM1g) shows the dike is ~10-km-long, has maximum opening of ~2.2±0.1 m, and that near surface normal faults slip by no more than 1.3 m. Most opening occurred between 3 - 8 km along strike, and between 2 - 8 km depth range, with little opening below 9 km or above 1 km. A total of 0.12±0.02 km^3 of magma was intruded, giving a geodetic moment of 3.7×10^{18} Nm.

Differences between observed (Fig. SM1a and d) and modeled deformation (Figs. SM1b and e) are plotted on residual interferograms (Fig. SM1c and f). The model explains most of the deformation with rms misfit to LOS data of 23 mm (Figs SM1c and f), comparable to the level of noise in the far-field (~20 mm). Larger misfits occur close to the dyke where data coherence is poor. The 1-σ errors are less than 22 cm throughout the model, with maximum errors occurring in regions of incoherence in the InSAR data (Fig. SM1h).

July 2006 dike

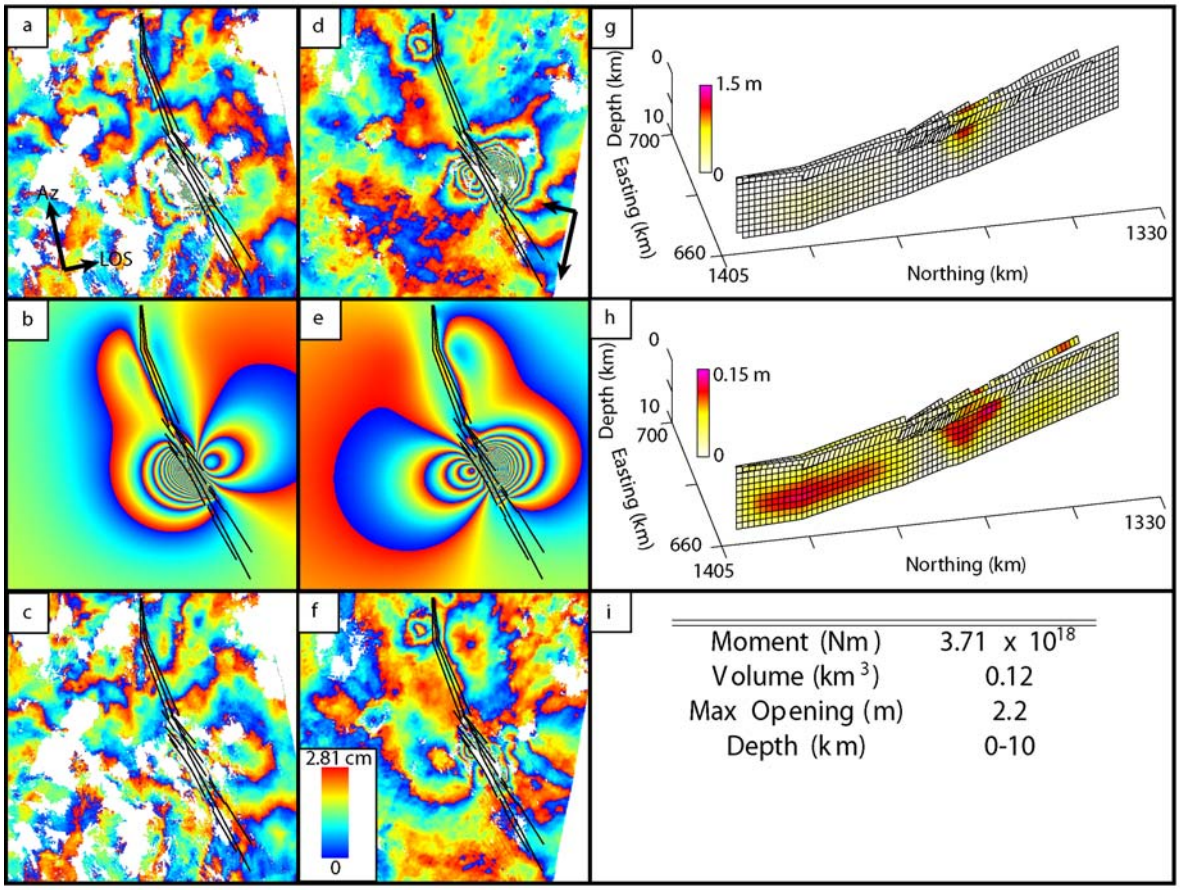

Figure SM2: Observed and modeled deformation for the July 2006 dike intrusion. a) observed, b) modeled, c) residual ascending interferograms. c) observed, d) modeled, e) residual descending interferograms, f) Best-fit dike model, h) 1-σ errors, i) dike statistics.

Ascending and descending 35-day interferograms covering the month of July show deformation from intrusion of a dike (Fig. SM2a, d). The ascending interferogram uses images acquired from track 300 on July17 and August 21, while the descending interferogram uses images from track 464 acquired on June 24 and July 29. The observed deformation field is lower in magnitude than the June 2006 dike but has a similar pattern. The best-fitting dike

model (Fig. SM2g) shows a ~9-km-long dyke intruding between 0 and 5 km depth range. Maximum opening of 1.1±0.1 m occurred in the middle of the dike and the near surface normal faults slipped by up to 1 m. A total volume of 0.07±0.02 km^3 was intruded, giving a geodetic moment of 2.20×10^{18} Nm. Differences between observed (Fig. SM2a and d) and modeled deformation (Figs. SM2b and e) are plotted on residual interferograms (Fig. SM2c and f). The model explains most of the observed deformation with an rms misfit of 19 mm. The 1-σ errors are less than 13 cm for the entire model (Fig. SM2h).

Continuous Global Positioning System (cGPS) methods

We process phase and pseudorange GPS data in single-day solutions using the GAMIT-GLOBK software. It uses double-differenced GPS phase measurements to estimate daily station coordinates, satellite state vectors, 7 tropospheric delay parameters per site and day, horizontal tropospheric gradients, and phase ambiguities using International GNSS Service (IGS) final orbits and earth orientation parameters. We apply elevation-dependent antenna phase center models following the tables recommended by the IGS, solid Earth, polar tide and ocean loading corrections following the International Earth Rotation Service (IERS) standards. We include all continuous GPS stations in Africa to tie station positions to the International Terrestrial Reference Frame (ITRF). For the purpose of this study, we implement the reference frame by tightly constraining the GPS orbits and IERS earth orientation parameters to the final IGS values and map site positions with respect to site DA60.

We also produced epoch-by-epoch (i.e. every 30 seconds) positions for the baseline between sites DA60 and DA25. We fix the GPS orbit to the precise IGS values and the position of DA60 to known a priori values and solve for DA25 position every 30 seconds and phase ambiguities using a Kalman filter technique.

Topographic map of the Ado'Ale Volcanic Complex (AVC)

The Ado'Ale Volcanic Complex (AVC) is a rifted silicic complex located in the middle of the Dabbahu segment (Fig. SM3). Detailed fault maps and topography of the AVC are documented in Rowland et al. (2007). The name of the volcano is controversial. We use a minor modification on "Ado'Ale" used by Lahitte et al. (2003). However, the volcanic complex is severely rifted resulting in numerous topographic peaks on both western and eastern sides of the rift axis, each named by local Afar people (Fig. SM3). Recent field excursions to the area found the most prominent topographic features of the AVC are Diyyilu ("Charcoal" in English) and Ado'Ale ("White Mountain" in English) on the eastern side of the rift axis. The main part of the western side of the AVC in named Gommoyta ("Hill" in English).

The attached photo is taken from 40.58^{o}E, 12.42^{o}N viewing SE toward the northeastern flank of the AVC (Fig. SM4). The prominent triangular peak offset to the left of center is Diyyilu. The region comprising the lower mound on the left side of the photo is named Damoma, beneath which the 17 June 2006 dike intruded.

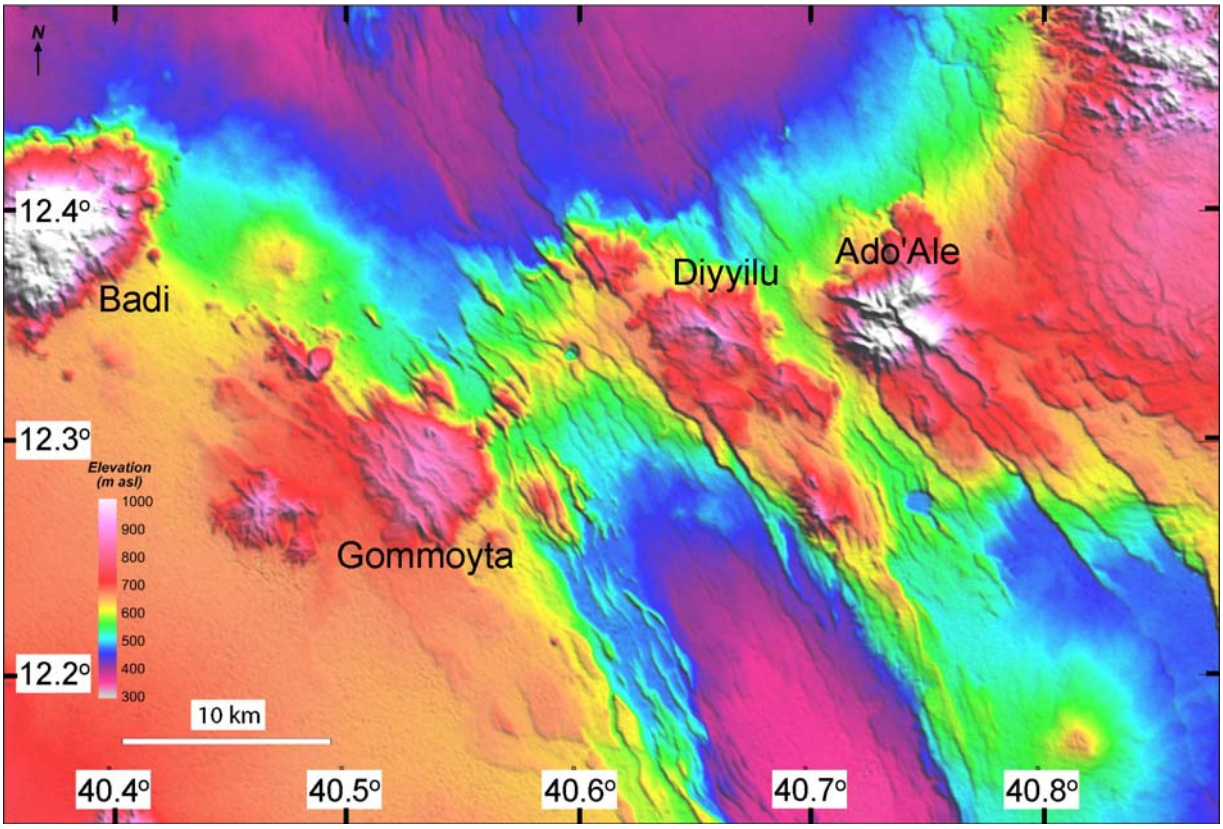

Figure SM3: Topography of the Ado'Ale Volcanic Complex (AVC) with names of prominent topographic peaks labeled.

Figure SM4: Field photograph taken from 40.58°E, 12.42°N and viewing SE toward the northeastern flank of the AVC. The prominent triangular peak offset to the left of center is Diyyilu.

References

Ebinger, C.J., Keir, D., Ayele, A., Calais, E., Wright, T.J., Belachew, M., Hammond, J.O.S., Campbell, M.E, and Buck, W.R., 2008, Capturing magma intrusion and faulting process during continental rupture: Seismicity of the Dabbahu (Afar) rift, Geophysical Journal International, v. 174, p. 1138-1152, doi: 10.111/j.1365-246X.2008.03877.x.

Farr, T. and Kobrick, M., 2000, Shuttle Radar Topography Mission produces a wealth of data, EOS Transactions, AGU, 81, 583,585.

Goldstein, R., Zebker, H., Werner, C., 1988, Satellite radar interferometry - Two-dimensional phase unwrapping, Radio Science (ISSN 0048-6604), vol. 23, p. 713-720.

Goldstein, R., Werner, C., 1998, Radar interferogram filtering for geophysical applications, Geophysical Research Letters, Volume 25, Issue 21, p. 4035-4038.

Gresta, S., Patanè, D., Daniel, A., Zan, L., Carletti, A., and Befekadu, O., 1997, Seismological evidence of active faulting in the Tendaho rift (Afar triangle, Ethiopia), Pure and Applied Geophysics, v. 149, p. 357-374.

Hamling, I.J., Wright, T.J., Ebinger, C.J., Keir, D., Lewi, E., Yirgu, G., 2008, InSAR observations of new dyke intrusion in the Dabbahu rift segment, Afar, Ethiopia, Geophysical Journal International, in review.

Hofstetter, R., and Beyth, M., 2003, The Afar Depression: Interpretation of the 1960-2000 earthquakes, Geophysical Journal International, v.155, p. 715-732.

Jónsson, S., Zebker, H., Segall, P., and Amelung, F., 2002, Fault Slip Distribution of the 1999 M_w 7.1 Hector Mine, California, Earthquake, Estimated from Satellite Radar and GPS Measurements, Bulletin of the Seismological Society of Americ, v. 92; no. 4; p. 1377-1389.

Keir, D., Stuart, G.W., Jackson, A., and Ayele, A., 2006, Local earthquake magnitude scale and seismicity rate of the northern Ethiopian rift, Bulletin of the Seismological Society of America, v. 96, p. 2221-2230, doi:10.1785/0120060051.

Lahitte, P., Gillot, P-Y., Courtillot, V., 2003, Silicic central volcanoes as precursors to rift propogation: the Afar case, Earth and Planetary Science Letters, v. 207, p. 103-116.

Makris, J., and Ginzburg, A., 1987, Afar Depression: Transition between continental rifting and sea-floor spreading, Tectonophysics, v. 141, p. 199-214.

Okada, Y., 1985, Surface deformation due to shear and tensile faults in a half-space, Bulletin of the Seismological Society of America, v. 75, p. 1135-1154.

Parsons, B., Wright, T., Rowe, P., Andrews, J., Jackson, J., Walker, R., Khatib, M., Talebian, M., Bergman, E., and Engdahl, E.R., 2006, The 1994 Sefidabeh (eastern Iran) earthquakes revisited: new evidence from satellite radar interferometry and carbonate dating about the growth of an active fold above a blind thrust fault, Geophysical Journal International, v. 164, p. 202-217.

Rosen, P.A., Hensley, S., Peltzer, G., and Simons, M., 2004, Updated repeat orbit interferometry package released, EOS Transactions, AGU, 85(5), 35.

Rowland, J. V., Baker, E., Ebinger, C. J., Keir, D., Kidane, T., Biggs, J., Hayward, N., and Wright, T. J., 2007, Fault growth at a nascent slow-spreading ridge: 2005 Dabbahu rifting episode, Afar, Geophysical Journal International, v. 171, p. 1226-1246.

Wright, T.J., Ebinger, C., Biggs, J., Ayele, A., Yirgu, G., Keir, D., and Stork, A., 2006, Magma-maintained rift segmentation at continental rupture in the 2005 Afar dyking episode, Nature, v. 442, p. 291-294.